Check for updates

Helical dinuclear 3d metal complexes with bis(bidentate) [S,N] ligands: synthesis, structural and computational studies†

Jamie Allen, [ID] [a] Jörg Saßmannshausen, [ID] [b] Kuldip Singh[a] and Alexander F. R. Kilpatrick [ID] *[a]

A diprotic bis(β-thioketoimine) ligand precursor featuring a flexible 4,4′-methylbis(aniline) linker, H$_2$**2**, was synthesised *via* treatment of the corresponding bis(β-ketoimine) with Lawesson's reagent. Lithiation of H$_2$**2** and coordination with one equivalent of d-block metal(II) chlorides MCl$_2$(THF)$_x$ (M = Fe, Co and Zn) yielded a corresponding series of homoleptic dinuclear complexes, [M$_2$(μ-**2**)$_2$]. X-ray diffraction analysis reveals a tetrahedral geometry for the two metals and a double-stranded helicate structure arising from inter-strand face-face π-stacking. These interactions create a helical 'twist' of *ca.* 70°. Utilising a bulky mononucleating β-thioketoiminate ligand, [**3**]$^-$, the analogous series of homoleptic monometallic complexes, [M(**3**)$_2$] (M = Fe, Co and Zn), were prepared and characterised by spectroscopic and analytical techniques. A comprehensive DFT study of all complexes reveals a stronger M−S bonding compared to M−N due to a higher degree of covalency. Solution magnetic studies and natural bonding orbital calculations on the mono- and dinuclear iron and cobalt complexes are consistent with high-spin tetrahedral Fe(II) and Co(II) centres, and cyclic voltammetry reveals both oxidation and reduction processes are accessible.

Introduction

Cooperative reactivity between multiple metal centres is well-known in heterogeneous catalysis, and many metalloproteins (such as photosystem II) use ensembles of metals in their active sites. The concept of cooperativity is increasingly being embraced in molecular catalysts, where pairs of metals can be used to direct reactivity, selectively, down one of many possible pathways.[1,2] Some metal-catalysed reactions feature a more reactive and selective bimetallic pathway between two individual catalytic units.[3] However, this intermolecular bimetallic activation can be inefficient, particularly at low catalyst loading, because of the low concentration of active bimetallic species. To overcome this limitation, synthetic chemists have developed a tethering strategy, in which two or more catalytic units are linked through an appropriate linker or merged within a single framework.[4]

One approach to this is the use of homoditopic ligands. Homoditopic ligands contain two identical metal-binding sites and are more straightforward to synthesise than heteroditopic ligands, which contain differentiated binding sites. While N, O and P-donor atoms are common in bidentate binding sites,[5–10] in both homo and hetero sets,[11] S-donors are relatively unexplored in this regard. Duboc and co-workers reported a bisamine alkyl dithiolate,[12–15] which upon oxidation forms a dinucleating bis[S,N,N] ligand that allows the stabilisation of two copper centres.[16] Hahn and co-workers reported a series of dinuclear and trinuclear complexes bearing Schiff-base ligands with two [S,N] binding sites, following a subcomponent self-assembly strategy with nickel or zinc as template metals.[17,18] Wu and co-workers employed a dinucleating ligand with two aminothiophenolate [S,N] binding domains separated by a rigid 1,3-bis(methylene)phenylene spacer to synthesise a higher-nuclear (Zn$_{10}$) circular helicate.[19]

Another possible [S,N] ligand framework is the *N*-aryl β-thioketoiminate ([SacNac^{Ar}]$^-$). There are a growing number of complexes reported with [SacNac^{Ar}]$^-$ ligands,[20] which have been proposed as interesting candidates for electrochemical and biological applications,[21–25] but have only recently attracted attention in catalysis.[26,27] SacNac^{Ar} ligands have until now not been incorporated into a dinucleating homoditopic ligand framework.

[a]School of Chemistry, University of Leicester, University Road, Leicester, LE1 7RH, UK. E-mail: sandy.kilpatrick@leicester.ac.uk

[b]Imperial College London, London, SW7 2AZ, UK

Our studies focus on novel dinucleating ligands in complexes with first-row transition metals, which are important in the drive towards using more benign and sustainable base metals in synthesis and catalysis.[28] Whilst the range of metals incorporated into β-thioketoiminate ligands has grown rapidly in recent years,[20] surprisingly, complexation with the majority of first-row transition metals remains unaddressed. Macrocyclic ligands featuring two N-linked β-thioketoiminate sites binding to a single metal centre are known,[29–31] but we were interested in extending this concept to bis (β-thioketoiminates) that can coordinate two metal centres in a bridging mode, for which there exists a knowledge gap. We took inspiration from Kretschmer's bimetallic indium(I) and gallium(I) complexes with bis(β-diketiminate) ligands, that show cooperative bond activation and reactivity towards small molecules.[33–35] However, in contrast to these main group systems, reactive low-valent transition metal centres are typically generated via reduction of metal(II) halide precursors.[36] Therefore we initially targeted heteroleptic complexes of the type [SacNac^{Ar}]M^{II}X (where X = monoanionic ligand), which are also attractive candidates for catalytic studies.

Herein, we report the synthesis of an acyclic homoditopic ligand featuring two isolated [S,N] binding sites and its corresponding dinuclear complexes with first-row 3d metals Fe, Co and Zn. The +2 oxidation state was employed in all cases to gauge how the metal centre affected the complex structures, electrochemical and magnetic properties.

Results and discussion

Synthetic studies

The linker group 4,4′-methylbis(aniline) was selected due to its flexibility, which can enable cooperativity between two metals, and allow for fine-tuning of the metal–metal distance and steric environment.[37–45] Rieger and co-workers previously reported a bis(β-ketoimine) derived from this linker, H$_2$1, as a ligand precursor to a dinuclear zinc hexamethyldisilylazane bis(β-diiminate) complex which showed high activity as a catalyst for ring opening co-polymerisation of cyclohexene oxide and CO$_2$.[46]

The most common synthetic route to N-aryl β-thioketoimine proligands, HSacNac^{Ar}, is the thionation of the corresponding β-ketoimine precursors with Lawesson's reagent (LR).[47,48] Following this precedent, conversion of H$_2$1 to H$_2$2 proceeded straightforwardly (Scheme 1), without the need for column chromatography, to afford the bis(bidentate) [S,N] proligand H$_2$2 in 71% yield.
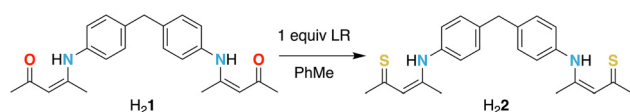
The structure of H$_2$2 was confirmed by ^{1}H and ^{13}C NMR spectroscopy in CDCl$_3$ and in the solid state by single crystal XRD. ^{1}H NMR spectroscopy reveals a resonance at 15.53 ppm in CDCl$_3$ (16.04 ppm in C$_6$D$_6$), assigned to the NH protons, which are more deshielded than the corresponding resonances in β-diketoimines and β-ketoimines (δ_H(CDCl$_3$)/ppm: 12.62 in HNacNac$^{p\text{-Tol}}$, H({4-MeC$_6$H$_3$NCMe}$_2$CH); 12.42 in HAcNac$^{p\text{-Tol}}$, 4-MeC$_6$H$_3$N(H)C(Me)CHC(O)Me).[49] Similar shifts for this environment are observed in related HSacNac^{Ar} proligands – Ar = Ph (15.56), 2,4,6-trimethylphenyl (Mes) = (15.33), 2,6-diisopropylphenyl (Dipp) = (15.30).[50] Three singlet signals in a 3 : 3 : 1 ratio are observed for the two inequivalent methyl groups and central β-CH protons of the HSacNac^{Ar} moiety, respectively. A characteristic deshielded C=S environment is observed at δ_C 207.5 ppm, in line with data reported for HSacNac^{Ar} proligands (Ar = Ph (207.6 ppm), Mes (205.9 ppm) and Dipp (206.9 ppm)).[50]

Single crystals of H$_2$2 were grown from a CH$_2$Cl$_2$ solution at room temperature. The structure determined by XRD (Fig. 1) shows a C–S distance (average 1.6875(3) Å) shorter than a typical C$_{sp2}$–S single bond (ca. 1.75 Å), but longer than a typical C=S double bond (ca. 1.67 Å),[51] suggesting intermediate bond order. The near-planarity of the S1–C1–C2–C3–N1 moiety (atom distances from mean plane = 0.004–0.017 Å) is consistent with a conjugated π-system. Protons H1 and H2 are closely associated with the N1 and N2 atoms, respectively, congruent with a typical N–H bond being stronger than a typical S–H bond. Collectively these observations are consistent with a protonated β-thioketoiminate tautomer (Scheme 1) as the best description of the form of H$_2$2 present in solution and the solid state, in keeping with López and co-workers description of mononucleating HSacNac^{Ar}; Ar = Ph, Mes and Dipp (=H(3)).[23,24,47,52]

Homoleptic complexes of divalent transition metals with this bis(bidentate) [S,N] ligand were readily accessed. Facile deprotonation of H$_2$2 with two equivalents of LiN(TMS)$_2$·THF afforded Li$_2$2, as evidenced by ^{1}H and ^{7}Li NMR spectroscopy (Fig. S3 and S4†). Salt metathesis reactions of Li$_2$2 with 1 equiv. of divalent metal halides FeCl$_2$(THF)$_{1.5}$, CoCl$_2$(THF)$_{1.5}$ and ZnCl$_2$ in THF, followed by extraction and recrystallisation
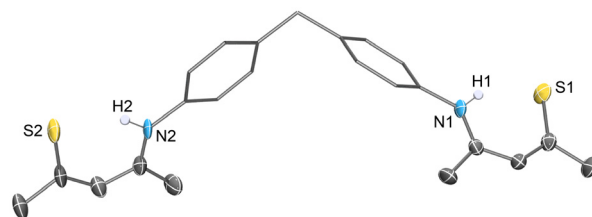

Fig. 1 Solid state molecular structure of H$_2$2 with ellipsoids at 50% probability (except for the aryl fragments shown in a wireframe). Hydrogen atoms (except H1 and H2) are omitted for clarity. Selected average bond distances (Å) and angles (°): N–C(α) = 1.3355(4); S–C(α) = 1.6875(3); C(N)–C(β) = 1.4015(4); C(S)–C(β) = 1.3905(4); N–C(α)–C(β) = 120.35(2); S–C(α)–C(β) = 126.21(12); C(α)–C(β)–C(α) = 129.55(3); C–CH$_2$–C = 112.35(18).

Scheme 1 Synthesis route to bis(β-thioketoimine) proligand H$_2$2.

in toluene in each case furnished the corresponding homoleptic complexes $[M_2(\mu\text{-}2)_2]$; M = Fe, Co and Zn (Scheme 2), which were characterised by NMR spectroscopy, mass spectrometry and single crystal XRD. A significant amount of coloured insoluble materials were formed in these reactions (in addition to colourless salt), which could not be extracted with toluene and as a result the isolated crystalline yields of the dinuclear complexes, $[M_2(\mu\text{-}2)_2]$; M = Fe, Co and Zn, were variable (3–57%). Furthermore, lower yields were obtained if the reaction mixture was stirred for longer. These observations may be explained by the possible formation of aggregated oligo/polymeric $[M(2)]_x$ species which have poor solubility in hydrocarbon solvents.

^{1}H and ^{13}C NMR data for crystalline samples of the zinc complex reveal at least two sets of signals, with VT NMR measurements in toluene-d_8 revealing no change in their relative integrations between 298–368 K. The major species shows a D_2 symmetric structure, consistent with the solid state structure of $[Zn_2(\mu\text{-}2)_2]$ determined by XRD (*vide infra*). Previous reports of analogous dinuclear helicate assemblies,[42,43] suggest possible minor species could be assigned to an isomer of $[Zn_2(\mu\text{-}2)_2]$ with C_{2h} symmetry (*vide infra*), or a higher nuclearity $[Zn(2)]_x$ species. High resolution mass spectrometry (HRMS) data show the parent ion for $[Zn_2(\mu\text{-}2)_2]$ (m/z = 917.1411 $[M + H]^+$), and evidence for higher m/z species, but no major signals that could be confidently assigned a trinuclear complex. $[Zn_2(\mu\text{-}2)_2]$ was alternatively prepared as a yellow microcrystalline solid in 23% yield, *via* protonolysis reaction of equimolar H$_2$**2** and ZnEt$_2$ in toluene. However, this sample showed the same two species by ^{1}H NMR spectroscopy and satisfactory elemental analysis could not be obtained.

^{1}H NMR spectra of $[M_2(\mu\text{-}2)_2]$; M = Fe and Co each show paramagnetically broadened and shifted peaks, ranging between 88 and −91 ppm for $[Fe_2(\mu\text{-}2)_2]$ (Fig. S5†) and between 54 and −65 ppm for $[Co_2(\mu\text{-}2)_2]$ (Fig. S6†). Elemental analysis data were acceptable for $[Fe_2(\mu\text{-}2)_2]$ with one toluene molecule of crystallisation, but satisfactory data could not be obtained for $[Co_2(\mu\text{-}2)_2]$. Therefore, HRMS measurements were performed for the latter complex (Fig. S15†), which showed a major peak for the expected parent ion.

Attempted synthesis of a heteroleptic di-Zn complex by treatment of Li$_2$**2** with two equivalents of ZnCl$_2$ was unsuccess-

ful, affording $[Zn_2(\mu\text{-}2)_2]$ as the major component identified by ^{1}H NMR spectroscopy. Furthermore, protonolysis reactions of H$_2$**2** with two equivalents of either ZnEt$_2$ or Zn(N{TMS}$_2$)$_2$ in toluene, revealed approximately equimolar amounts of $[Zn_2(\mu\text{-}2)_2]$, ethane or HN(TMS)$_2$, and unreacted ZnEt$_2$ or Zn(N{TMS}$_2$)$_2$, respectively. Thus, it can be concluded that homoleptic $[Zn_2(\mu\text{-}2)_2]$ is the thermodynamic product. The two [S,N] binding pockets in ligand $[\mathbf{2}]^{2-}$ are disposed too far apart to coordinate a single Zn centre simultaneously, and instead two ligands each coordinate two metal centres in a bridging mode. The latter binding mode has also been observed in dinuclear alkaline earth,[53–56] rare earth,[57] iron,[58] and zinc[59] complexes with related dinucleating ligands with monoanionic $[N,N']$ binding sites. Yoshida and co-workers utilised a bis-bidentate $[N,O]$ Schiff base ligand to synthesise several supramolecular motifs, including a Zn$_2$L$_2$ double-stranded helicate.[60] Hahn and co-workers reported a subcomponent self-assembly route to Co$_2$, Ni$_2$, Zn$_2$ and Pd$_2$ dinuclear complexes bearing Schiff-base ligands with two [S,N] binding sites, using nickel or zinc as template metals.[17,18] In the case of the zinc complex, an equilibrium was observed between the dinuclear and trinuclear species, evidenced by ^{1}H NMR and mass spectrometry.

The synthetic problems associated with variable yield of dinuclear complexes $[M_2(\mu\text{-}2)_2]$ (M = Fe, Co, Zn) and bulk purity of the Co$_2$ and Zn$_2$ species, prompted investigation of mononuclear analogues, to better understand the synthesis, structure and bonding of Fe(II), Co(II) and Zn(II) in SacNac^{Ar} complexes. Utilising the bulky β-thioketoimine ligand, SacNac^{Dipp} = $[MeC=SCHC=N\{Dipp\}Me]^-$ (**3**), complexes $[M(3)_2]$ for M = Fe, Co, Zn were prepared according to Scheme 3. These were isolated in fair yields (34–59%) and characterised by NMR spectroscopy, elemental analysis, and single crystal XRD. Solution NMR data for diamagnetic $[Zn(3)_2]$ shows 12 resonances in the ^{1}H spectrum, and 17 resonances in the ^{13}C spectrum (Fig. S11 and S12†). ^{1}H NMR spectra of $[M(3)_2]$; M = Fe and Co also show 12 signals which are paramagnetically broadened and shifted (Fig. S8–S10†). These observations are consistent with two SacNac^{Dipp} ligands that are equivalent on the NMR timescale, each with axial chirality and restricted rotation about the N–Ar bond giving rise to complete inequivalence of all magnetic environments in the Dipp group.
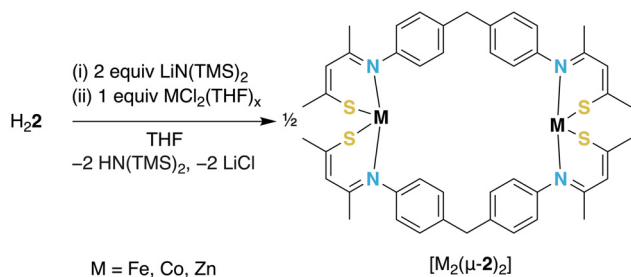
Scheme 2 Synthesis route to dinuclear complexes $[M_2(\mu\text{-}2)_2]$ for M = Fe, Co, Zn.

Scheme 3 Synthesis route to mononuclear complexes $[M(3)_2]$ for M = Fe, Co, Zn.

Structural studies

The solid state structures of $[M_2(\mu\text{-}2)_2]$ and $[M(3)_2]$ for M = Fe, Co and Zn were determined by single crystal XRD (Fig. 2, 3 and Table 1). Dinuclear complexes in each case show two metal(II) centres framed by two bis(β-thioketoiminate) ligands in a double-stranded helicate structure.[61] The two near-tetra-

Fig. 2 Solid state molecular structures of (top to bottom): $[Fe_2(\mu\text{-}2)_2]$, $[Co_2(\mu\text{-}2)_2]$, and $[Zn_2(\mu\text{-}2)_2]$, with ellipsoids at 50% probability (except for the aryl fragments shown in a wireframe). Hydrogen atoms are omitted for clarity. The complexes have crystallographically-imposed two-fold symmetry.

hedral metal centres ($\tau_4 = 0.90$),[62] are each bound by two bidentate [S,N] moieties, which results in two centres of axial chirality (Fig. S31†). The crystal structures reveal homochirality at each metal centre, Fig. 2 shows $[Fe_2(\mu\text{-}2)_2]$ and $[Zn_2(\mu\text{-}2)_2]$ in Δ,Δ configuration and $[Co_2(\mu\text{-}2)_2]$ in Λ,Λ configuration. However, extended views of the crystal packing (Fig. S24–S26†) reveal that each compound crystallises as the racemate, as expected for an achiral ligand **2**. The "twist" of the helix, defined by the torsion angle between two S–M–S mean planes is 71.88(5)° for $[Fe_2(\mu\text{-}2)_2]$, 69.50(4)° for $[Co_2(\mu\text{-}2)_2]$, and 68.23(7)° for $[Zn_2(\mu\text{-}2)_2]$. The helix is screwed clockwise (*P*) in the Δ,Δ structures and anticlockwise (*M*) in the Λ,Λ structures. In each case, the aryl rings of one linker unit are aligned near-coplanar with the aryl rings of the second linker unit (angle between mean planes 6.49(16)°–10.5(2)°), stacked offset with an inter-ring centroid–centroid distance of *ca.* 4.1 Å (range: 4.154–4.095 Å), suggesting the helical structure is stabilised by intramolecular (inter-strand) π–π interactions.[18,44,63]

The mononuclear structures, $[M(3)_2]$ for M = Fe, Co, Zn, also show near-tetrahedral geometry about the metal centres ($\tau_4 = 0.80–0.87$). This is in contrast to homoleptic Fe^{II} complexes of bulky β-ketoiminate ligands which tend towards a seesaw geometry/distorted trigonal-pyramidal geometry, showing τ_4 values in the range 0.53–0.56.[52,64–66] Bond metrics about the Fe, Co and Zn centres are also similar within the three mononuclear structures, $[M(3)_2]$: $d(\text{M–N})^{av}$ range: 2.05835–2.0035 Å, $d(\text{M–S})^{av}$ range: 2.28735–2.2449 Å, and compare well with those reported previously for high spin Fe(II),[67–69] and Co(II) complexes, and comparable zinc complexes.[18,29,68,70]

Comparison between $[M_2(\mu\text{-}2)_2]$ and $[M(3)_2]$ for each metal reveals smaller angles N–M–N angles for the dinuclear complexes compared with their mononuclear counterparts, which may be explained by π–π interactions of the two *N*-aryl rings in two linker groups causing a 'tethering' effect.

Mononuclear complexes $[M(3)_2]$ show differentiated ligands in the solid state, in contrast to the equivalent ligands on the NMR timescale observed in solution. For example, inspection of the metrical parameters for $[Co(3)_2]$ (Table S6†) reveals two

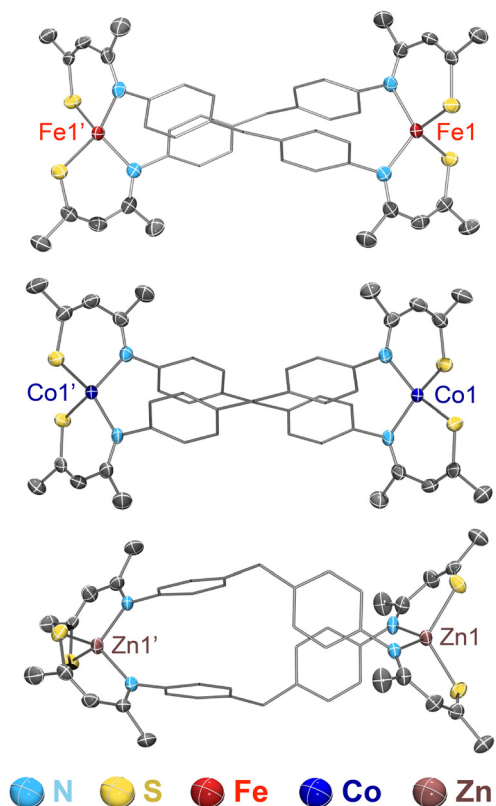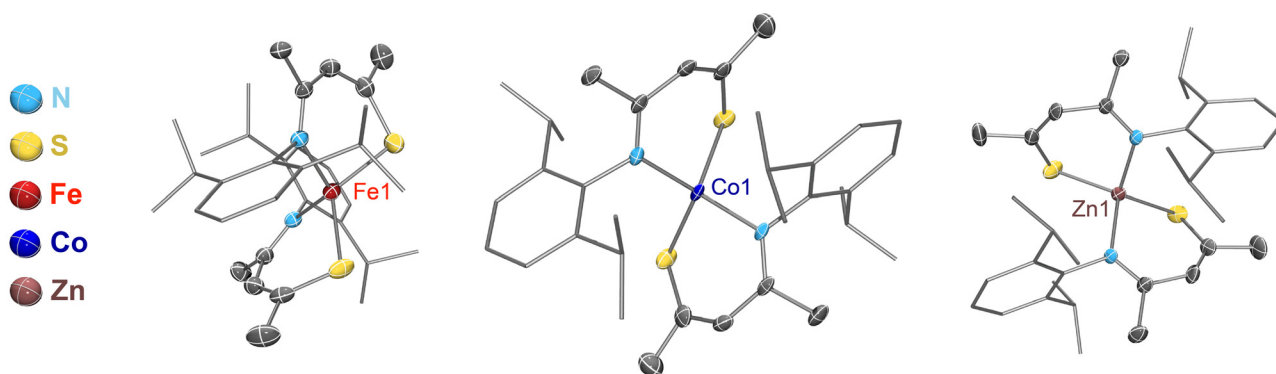**Fig. 3** Solid state molecular structures of (left to right): $[Fe(3)_2]$, $[Co(3)_2]$, and $[Zn(3)_2]$, with ellipsoids at 50% probability (except for the aryl fragments shown in a wireframe). Hydrogen atoms are omitted for clarity.

Table 1 Selected structural parameters, distances (Å) and angles (°) determined by XRD for $[M_2(\mu\text{-}\mathbf{2})_2]$ and $[M(\mathbf{3})_2]$; M = Fe, Co, and Zn

	$[Fe_2(\mu\text{-}\mathbf{2})_2]$	$[Fe(\mathbf{3})_2]$	$[Co_2(\mu\text{-}\mathbf{2})_2]$	$[Co(\mathbf{3})_2]$	$[Zn_2(\mu\text{-}\mathbf{2})_2]$	$[Zn(\mathbf{3})_2]$
M···M	11.7274(12)	—	11.8649(13)	—	12.0073(17)	—
Twist	71.88(5)	—	69.50(4)	—	68.23(7)	—
M–S^{av}	2.3049(13)	2.2874(9)	2.2575(11)	2.2449(11)	2.2899(18)	2.2647(7)
M–N^{av}	2.0085(3)	2.0558(14)	1.9805(3)	2.0035(2)	2.0355(3)	2.0584(13)
S–M–S	115.91(5)	125.3(3)	117.25(4)	116.03(4)	118.49(6)	125.23(4)
N–M–N	115.90(13)	121.34(6)	111.90(12)	121.89(11)	109.21(18)	115.99(6)
N–M–S^{av}	106.61(8)	103.12(6)	107.12(9)	105.005(9)	107.40(15)	104.18(5)
τ_4	0.90	0.80	0.90	0.87	0.90	0.84
Fold^{av}	20.25(15)	34.79(8)	21.86(14)	34.76(12)	25.00(2)	33.37(7)
C–CH$_2$–C	117.1(4)	—	117.4(4)	—	116.9(6)	—
Ar···Ar	4.154(2)	—	4.147(3)	—	4.095(4)	—

fold angles (angle between the N–M–S mean plane and the ligand backbone mean plane) for the two coordinated SacNac^{Ar} ligands that are significantly different in the XRD structure (29.26(12)° and 40.26(12)°), and an even greater difference in fold angles in the DFT calculated structures (26.0° and 40.9°, *vide infra*). The analogous di-cobalt complex $[Co_2(\mu\text{-}\mathbf{2})_2]$ shows no significant differences in the coordinated β-thioketoiminate moieties (fold angles = 21.15(14)° and 22.57(14)°).

Cini *et al.* and Hewlins have reported first-row 3d metals with a N_2S_2 donor set from tetradentate *N,N′*-alkyl bridged bis (β-thioketoiminate) ligands,[29–31] and Takihrov *et al.* reported a homoleptic zinc complex with a related bidentate [S.N] ligand [PhC=SC{^{i}Pr}C=N{Cy}H]$^-$.[32] However, to our knowledge, $[M_2(\mu\text{-}\mathbf{2})_2]$ and $[M(\mathbf{3})_2]$ are the first crystallographically characterised Fe(II), Co(II) and Zn(II) complexes supported by bidentate SacNac^{Ar} ligands.

Electrochemical and magnetometry studies

The redox properties of $[M_2(\mu\text{-}\mathbf{2})_2]$ and $[M(\mathbf{3})_2]$ (M = Fe, Co and Zn) were investigated by cyclic voltammetry in 0.1 M [^{n}Bu$_4$N][PF$_6$]/THF (Fig. 4). Dinuclear complexes $[M_2(\mu\text{-}\mathbf{2})_2]$ each

Fig. 4 CV scans (1 cycle) of $[M_2(\mu\text{-}\mathbf{2})_2]$ in THF/0.1 M [^{n}Bu$_4$N][PF$_6$], scan rate 100 mV s^{-1}. Current axes have been offset and normalised for comparison purposes.

showed a reductive event (process I) with a mid-peak potential ($E_{\frac{1}{2}} = \{E_{pa} + E_{pc}\}/2$) of −2.36, −2.04 and −2.44 V *vs.* FeCp$_2^{+/0}$, for Fe$_2$, Co$_2$, and Zn$_2$, respectively. Process I observed for $[M(\mathbf{3})_2]$ is more irreversible in comparison (Fig. S19 and Table S1†), but shows a similar trend in cathodic peak potential (E_{pc}) values of −2.69, −2.37 and −3.06 V *vs.* FeCp$_2^{+/0}$, for Co, Fe and Zn, respectively. Process I is tentatively assigned to a ligand-based reduction on the basis of comparable values.[71] Scanning to positive potentials revealed an oxidative feature for the iron and cobalt complexes, classified as irreversible (E_{pa} = 0.20 V for $[Fe_2(\mu\text{-}\mathbf{2})_2]$) and quasi-reversible ($E_{\frac{1}{2}}$ = −0.04 V for $[Co_2(\mu\text{-}\mathbf{2})_2]$), respectively. We assign the latter to a metal-based oxidation, where a negligible to unrecognisable interaction between metal centres leads to a class I mixed-valent situation.[72] Oxidation process II for monometallic $[Fe(\mathbf{3})_2]$ is irreversible (E_{pa} = 0.19 V) with no associated reduction (Fig. S19 and Table S2†), and for $[Co(\mathbf{3})_2]$ an oxidation (E_{pa} = 0.32 V) with an associated reduction was observed (E_{pc} = −0.38 V) that did not meet the criteria for a reversible process. It is noteworthy that the redox processes in the dimetal complexes show more reversibility than those of the corresponding mononuclear complexes, possibly indicating additional stability in the oxidised/reduced forms in the helicate structure.

CV data previously reported by Mehn and co-workers for the related mononuclear homoleptic β-ketoiminate complexes Co(L)$_2$ (L = [MeC=OCHC=N{Ar}Me]$^-$) show a Co^{II}/Co^{III} oxidation that is irreversible for Ar = Ph (E_{pa} +0.255 V), while the corresponding complexes with Ar = Mes and Dipp, exhibit a quasi-reversible one-electron oxidation ($E_{\frac{1}{2}}$ = +0.32 V and −0.70 V, respectively).[6] Previously reported CV data for the related mono-iron β-ketoiminate complexes Fe(L)$_2$ show quasi-reversible one-electron oxidation waves at $E_{\frac{1}{2}}$ = −0.185 V (Ar = ^{i}Pr) and −0.245 V (Ar = Dipp).[52] The corresponding mono-zinc β-ketoiminate complexes Zn(L)$_2$ also show irreversible oxidative and quasi-reversible reductive waves, which were ascribed to ligand oxidation and reduction, respectively. However, direct comparisons should be treated with a degree of caution due to the different supporting electrolyte systems used by Mehn and co-workers (0.4 M [^{n}Bu$_4$N][ClO$_4$]/THF) and in the present study (0.1 M [^{n}Bu$_4$N][PF$_6$]/THF).

Solution magnetic susceptibility measurements for all paramagnetic complexes were carried out using the Evans NMR
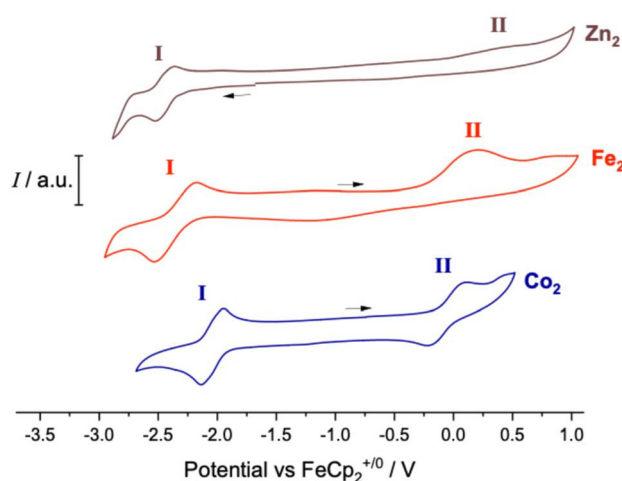
Table 2 Effective magnetic moment per metal for $[M(3)_2]$ and $[M_2(\mu\text{-}2)_2]$; M = Fe, Co

Complex	μ_{eff}(soln)/μ_B per M
$[Fe_2(\mu\text{-}2)_2]$	4.64
$[Fe(3)_2]$	4.58
$[Co_2(\mu\text{-}2)_2]$	3.85
$[Co(3)_2]$	3.83

method (Table 2).[73,74] The effective magnetic moments per iron centre are within error for bimetallic $[Fe_2(\mu\text{-}2)_2]$ (4.64μ_B) and monometallic $[Fe(3)_2]$ (4.58μ_B) complexes. These values are slightly lower than the calculated spin-only value for high-spin iron(II) (4.90μ_B), but comparable to the value 4.5(1)μ_B for the similar tetrahedral iron(II) bis(imidoyl aminothiolato) complex, $[Fe(MesC\{N^iPr\}\{N^iPrS\})_2]$, reported by Deng and co-workers.[75] Similarly, the effective magnetic moments per cobalt for $[Co_2(\mu\text{-}2)_2]$ (3.85μ_B), and $[Co(3)_2]$ (3.83μ_B) are self-consistent, but slightly lower than the calculated spin-only value for high-spin cobalt(II) (3.88μ_B) ions, and lower than values reported for other tetrahedral Co bis(bidentate) [S,N] complexes (4.8–4.88μ_B).[76,77]

DFT studies

Further information about the nature of the electronic structures of $[M_2(\mu\text{-}2)_2]$ and $[M(3)_2]$ (M = Fe, Co, Zn) was investigated by means of DFT calculations at the PBE0-D3/Wachters(Fe), SDD(Co, Zn), 6-311G(d,p) (C, H, N, S) level of theory,[78,79] in line with a recent benchmarking report on similar transition metal compounds.[80–82]

The DFT optimised geometries were in good agreement with those found by XRD (Tables S5–S10†), with similar average metrical parameters in the primary coordination sphere of the metal: e.g. for $[Fe_2(\mu\text{-}2)_2]$ Fe–S^{av} = 2.3228 Å; Fe–N^{av} = 2.0304 Å; Fe···Fe = 11.3316 Å; ring dihedrals = 88.68; τ_4 = 0.89. Differences were observed in the fold angles for $[Fe_2(\mu\text{-}2)_2]$ (angle between the N–M–S mean plane and the ligand backbone mean plane) for the two β-thioketoiminate ligands coordinated to each metal, which are differentiated in the DFT structure (12.53° and 21.94°), but similar in the XRD structure (19.77(15)° and 20.25(15)°). Similar observations can made for all structures, and these differences could originate from crystal packing effects.

Slight differences in the macrocyclic ligand backbone are observed between the experimental and calculated structures. For example, for $[M_2(\mu\text{-}2)_2]$ structures the angle between the bridging carbon and the tethered aryl rings, Ar–CH$_2$–Ar, is more acute for the calculated compared with the experimental structures (M = Zn: 115.64° – calc. vs. 116.88° – exp.; Fe: 115.39° – calc. vs. 117.12° – exp.; Co: 115.49° – calc. vs. 117.45° – exp.). One possible explanation is 'pressure' from the surrounding molecules in the solid state, which forces the macrocycle into a slightly more bent conformation. However, a certain degree of error within the calculated structures cannot be ruled out.

Given the NMR and XRD data for $[Zn_2(\mu\text{-}2)_2]$ are consistent with homochiral configurations at the zinc centres (rac = Δ,Δ or Λ,Λ), the (non-observed) meso isomer with opposite configurations at each zinc centre (Δ,Λ) was modelled. The DFT optimised structure (Fig. S38†) shows each Zn centre has opposite chirality (Δ,Λ) and whilst $[2]^{2-}$ bridges two different Zn centres, the ligands do not "twist" and rather coordinate in a "side to side" arrangement (twist angle 6.7°), giving a double stranded meso-helicate. The calculated structure of rac-$[Zn_2(\mu\text{-}2)_2]$ (Fig. S34†) shows near-parallel off-centred stacking between aryl rings (inter-ring centroid–centroid distance = 3.42 Å, mean plane-mean plane angle = 16.2°) whereas meso-$[Zn_2(\mu\text{-}2)_2]$ shows near-perpendicular edge-to-face (CH···π) interactions (nearest CH to aromatic plane distance = 2.44 Å, mean plane-mean plane angle = 99.7°). The extent of intra-molecular (inter-strand) π–π interactions can be a determining factor in the relative stability of double-stranded helicates.[83–86] The DFT-calculated energy of rac-isomer $[Zn_2(\mu\text{-}2)_2]$ is 8.52 kJ mol^{-1} lower than the value calculated for the hypothetical meso-isomer, which could explain the structure observed by XRD and NMR.

Molecular orbital calculations using PBE0/SPKrDZC (Fig. 5 and Fig. S39–S74†) for closed shell Zn complexes $[Zn(3)_2]$ and $[Zn_2(\mu\text{-}2)_2]$ (Fig. S39–S44†) reveal that the HOMO and LUMO are ligand based. For the open shell complexes $[M(3)_2]$ and $[M_2(\mu\text{-}2)_2]$ (M = Fe, Co) structures the pictures are more complex. Whereas for $[Co(3)_2]$ the SOMOs are primarily metal based, this is not the case for $[Co_2(\mu\text{-}2)_2]$ where the SOMOs are more delocalised between the metal and the ligand. For $[Fe(3)_2]$ the SOMOs are more located at the S atom, with some contribution from the metal as well. This feature is also echoed in $[Fe_2(\mu\text{-}2)_2]$ where, somewhat similar to $[Co_2(\mu\text{-}2)_2]$, the SOMOs are more closely located at the S and metal atoms. To validate our findings, the calculations were repeated for $[Co(3)_2]$ and $[Fe(3)_2]$ using the Becke-Half-and-Half-LYP (BHandHLYP) functional, which contains 50% Hartree–Fock, instead of PBE0 and essentially the same orbitals were obtained (Fig. S71–S85†).

The spin density was obtained from Natural Bonding Orbital (NBO) calculations summarised in Table 3 for $[M(3)_2]$ and $[M_2(\mu\text{-}2)_2]$; M = Fe, Co (see ESI† for the complete set). The majority of the spin density is located at the metal centre for both mononuclear and dinuclear Co and Fe structures, and the S donor atoms have a higher spin density compared to N. This is also observed in the plots of the SOMO orbitals, indicating a certain degree of covalency for the M–S bonds. Hence, calculations are in agreement with C–S single bond character observed in the solid state structures, with S bonding as a thiolate to the metal, as opposed to a C=S double bond which would give a strictly dative M–S bond.

Further corroboration of these results was obtained from the Wiberg bond indices (WBI), and the results are summarised in Table 4. These data are in keeping with the results of the spin density calculations: the higher spin on sulfur results in a higher WBI, indicating a stronger interaction. This effect seems to be independent of the metal centre, since the closed
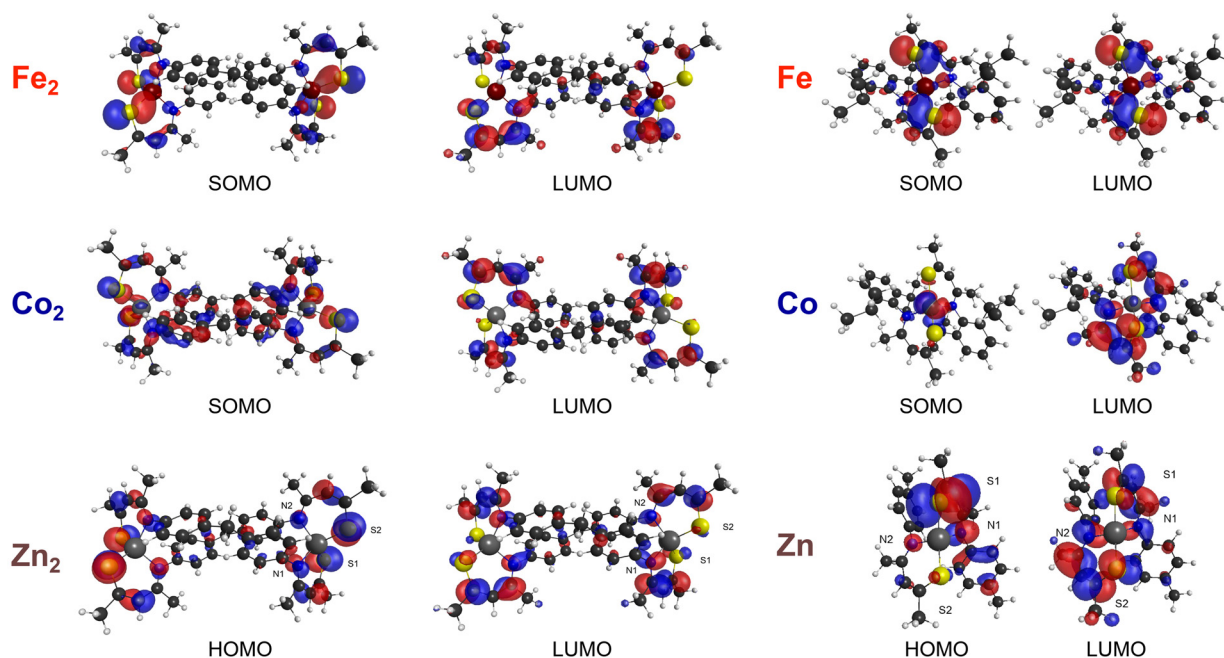
Fig. 5 Selected orbitals of $[M_2(\mu\text{-}2)_2]$ (left) and $[M(3)_2]$ (right); M = Fe, Co, and Zn.

Table 3 Spin densities as obtained by NBO for $[M(3)_2]$ and $[M_2(\mu\text{-}2)_2]$; M = Fe, Co

	$[Co(3)_2]$	$[Co_2(\mu\text{-}2)_2]$	$[Fe(3)_2]$	$[Fe_2(\mu\text{-}2)_2]$
M	2.53974	2.55082	3.57818	3.59190
S1	0.12033	0.13510	0.12780	0.13338
S2	0.12255	0.13530	0.12780	0.13259
N1	0.07272	0.08414	0.07235	0.07850
N2	0.07344	0.08293	0.07235	0.08007

Table 4 Selected computational data for $[M_2(\mu\text{-}2)_2]$ and $[M(3)_2]$ and M = Fe, Co, Zn

Structure	Bond	Distance[a]/ (Å)	WBI[b]	$\rho(\boldsymbol{r})$[c]	$\nabla^2\rho(\boldsymbol{r})$[d]	$G(\boldsymbol{r})/\rho(\boldsymbol{r})$[e]
$[Fe_2(\mu\text{-}2)_2]$	M–S^{av}	2.323	0.438	0.075	0.163	0.86
	M–N^{av}	2.030	0.270	0.091	0.343	1.26
$[Fe(3)_2]$	M–S^{av}	2.316	0.439	0.087	0.082	0.72
	M–N^{av}	2.056	0.242	0.082	0.341	1.24
$[Co_2(\mu\text{-}2)_2]$	M–S^{av}	2.289	0.442	0.078	0.179	0.92
	M–N^{av}	2.000	0.269	0.094	0.367	1.32
$[Co(3)_2]$	M–S^{av}	2.588	0.425	0.078	0.172	0.90
	M–N^{av}	2.023	0.247	0.084	0.382	1.35
$[Zn_2(\mu\text{-}2)_2]$	M–S^{av}	2.296	0.294	0.075	0.159	0.84
	M–N^{av}	2.032	0.129	0.083	0.372	1.21
$[Zn(3)_2]$	M–S^{av}	2.278	0.312	0.080	0.147	0.79
	M–N^{av}	2.046	0.117	0.079	0.324	1.23

av = averaged values. [a] DFT optimised geometry. [b] Wiberg bond index. [c] Electron density at bond critical point. [d] Laplacian of electron density at bond critical point. [e] Lagrangian kinetic energy per electron (in a.u.).

shell Zn structures show the same trends as the paramagnetic structures: the M–S bond has a higher WBI compared to the M–N one.

To further illustrate the points of the NBO, Wiberg and orbital analysis, QTAIM values for all complexes were calculated. The electron density of the bond critical points $[\rho(\boldsymbol{r})]$ between the metal and S and N (Table 4), respectively, do not provide much insight. In nearly all cases this value is around 0.08 with some minor deviations. Based on that computed parameter alone, the M–S and M–N bonds cannot be distinguished. However, the Laplacian of the electron density at the bond critical points $[\nabla^2\rho(\boldsymbol{r})]$ is more informative, revealing an average value of 0.15 for the M–S bonds compared with a more positive average value of 0.35 for M–N bonds. The values of $\nabla^2\rho(\boldsymbol{r})$ are quite consistent throughout the series, with Fe–S bond in $[Fe(3)_2]$ as the only exception. Energy density, $H(\boldsymbol{r})$, values are negative for all M–S and M–N interactions (Tables S11–S16†), consistent with a significant sharing of electrons.[87] The ratio $G(\boldsymbol{r})/\rho(\boldsymbol{r})$ defines the local kinetic energy per electron; values of this ratio lower than unity are associated with covalent-type interactions, while values greater than 1 are characteristic of ionic-type interactions. For both $[M_2(\mu\text{-}2)_2]$ and $[M(3)_2]$ complexes the $G(\boldsymbol{r})/\rho(\boldsymbol{r})$ values indicate more covalency in the M–S interactions, compared with more polar M–N interactions. Coloured plots of the electron density map, the Laplacians and the virial map are provided in the ESI (Fig. S87–S98†).

In summary, from the calculated, consistent metrics, we can conclude the M–S bond is the more dominant one compared with the M–N bond. This is indicated by the location of the spin density with S having nearly twice as much as N, together with the Wiberg bond indices and the Laplacians of the electron densities. These results are complementary to a computational studies by Phillips and co-workers, describing the bonding in η^6-arene Ru(II) and Os(II) β-diketoiminate and

β-thioketoiminate complexes.[50] Charge decomposition analysis revealed the β-thioketoiminate ligand as not only a strong σ- and moderate π-donor, but also significant back donation/ charge transfer from metal to sulfur, due to the better electron accepting properties of S compared with N.

Conclusions

We report the synthesis of a bis(bidentate) ligand, with isolated [S,N] binding sites interconnected by a flexible 4,4′-methylbis(aniline) linker group, and an isostructural series of dinuclear complexes with Fe(II), Co(II) and Zn(II) ions. In each case, neutral homoleptic complexes were formed, $[M_2(\mu\text{-}2)_2]$, in which the two metal centres are framed by two bis(β-thioketoiminate)s and show tetrahedral coordination geometry. However, yields and purity of the bimetallic complexes were variable, and therefore monometallic analogues with the bulky SacNac^{Dipp} ligand $[3]^-$ were synthesised for comparative purposes, which gave improved yields and microanalyses. XRD structures of $[M(3)_2]$ showed the SacNac^{Dipp} ligand binding in the expected κ²-[S,N] mode with near-tetrahedral geometry at the metal centres. NMR data for $[M(3)_2]$ revealed equivalent SacNac^{Dipp} ligands on the NMR timescale, and CV and solution magnetometry data were consistent with their bimetallic counterparts. This suggests the inferior purity of $[M_2(\mu\text{-}2)_2]$ is a result of the dinucleating ligand framework causing the formation of other species (possibly higher oligomers), rather than the β-thioketoiminate sites binding to the metal centres in an unusual manner. To our knowledge, $[M(3)_2]$; M = Fe, Co, and Zn, represent the first examples of crystallographically characterised complexes of these metals with SacNac^{Ar} ligands.

X-ray diffraction analysis reveals that the dinuclear structures $[M_2(\mu\text{-}2)_2]$; M = Fe, Co, and Zn, are twisted in the solid state, exhibiting helical chirality. This is attributed to intramolecular π–π stabilisation interactions between the aryl rings of the linker group in one ligand with those of the second ligand on the opposite side of the macrocycle.

Solution magnetometry studies of paramagnetic complexes $[Fe_2(\mu\text{-}2)_2]$, $[Fe(3)_2]$, $[Co_2(\mu\text{-}2)_2]$, and $[Co(3)_2]$ are consistent with high-spin configurations at each metal centre (S = 2 for Fe^{II}; S = 3/2 for Co^{II}). As expected, the large metal–metal separations of *ca.* 12 Å in $[Fe_2(\mu\text{-}2)_2]$ and $[Co_2(\mu\text{-}2)_2]$, precludes any intramolecular magnetic interactions. Hence, with a view on cooperative effects these complexes are classed as linked bimetallics, effectively two monometallic complexes tethered together, rather than twinned bimetallics where the two metals are in close enough proximity for direct metal–metal interactions to occur.

Given the facile accessibility of ligand $[2]^{2-}$ in good yields and its straightforward metalation, it is poised to attract further attention for the synthesis of new dinuclear coordination complexes in which mixed hard–soft donor groups are desirable. Considering the widespread utility of β-diketiminates in reactivity studies and catalysis, alongside the importance of sulfur-based ligands in metalloenzymes, the bis(β-thioketoiminate) ligand offers a new platform for the development of base-metal bimetallic catalysis and bio-inorganic studies.

Experimental section

Synthesis and characterisation of H$_2$2

To solution of H$_2$1 (5.00 g, 13.79 mmol) in toluene (100 mL) was added Lawesson's reagent (5.58 g, 13.79 mmol), giving a yellow suspension which was stirred for 1 h. The resultant red-brown mixture was filtered and the solvent removed from the filtrate giving an orange residue. Trituration with Et$_2$O (50 mL) afforded the title compound as an orange powder. Total yield: 3.87 g, 9.78 mmol (71%).

^{1}H NMR (400 MHz, CDCl$_3$, 298 K): δ_H 15.53 (br, $\Delta\nu_{\frac{1}{2}}$ = 45 Hz, 2H, NH), 7.22 (d, $^3J_{HH}$ = 8.5 Hz, 4H, Ar-CH), 7.14 (d, $^3J_{HH}$ = 8.5 Hz, 4H, Ar-CH), 6.27 (s, 2H, β-CH), 4.01 (s, 2H, CH_2), 2.61 (s, 6H, α-SCCH_3), 2.11 (s, 6H, α-NCCH_3). ^{13}C{^{1}H} NMR (100.5 MHz, C$_6$D$_6$, 298 K): δ_C 207.5 (C=S), 163.6 (α-NCCH$_3$), 139.7 (Ar C_Q–N), 135.6 (Ar C_Q–CH$_2$), 129.9 (Ar CH), 125.5 (Ar CH), 114.0 (β-CH), 41.0 (CH$_2$), 39.1 (α-SCCH$_3$), 21.5 (α-NCCH$_3$). HRMS (ESI) m/z calcd for C$_{23}$H$_{27}$N$_2$S$_2^+$: 395.1616 $[M]^+$; found: 395.1608. Anal. found (calcd for C$_{23}$H$_{27}$N$_2$S$_2$): C, 69.48 (70.01); H, 6.25 (6.64); N, 6.42 (7.10). Satisfactory elemental analysis could not be obtained despite repeated attempts on freshly prepared samples, so data ±0.6% are reported. IR (ATR): ν 2920, 2850, 1598, 1567, 1505, 1454, 1376, 1291, 1260, 1213 cm^{-1}.

Synthesis and characterisation of $[Fe_2(\mu\text{-}2)_2]$

A Schlenk flask was charged with H$_2$2 (150 mg, 0.38 mmol) and LiN(TMS)$_2$·THF (192 mg, 0.80 mmol). THF (5 mL) was added at −78 °C, affording a yellow-orange suspension which was allowed warm to room temperature and stir for 1 h. The mixture was transferred *via* cannula to a pre-cooled −78 °C suspension of FeCl$_2$·THF$_{1.5}$ (94 mg, 0.40 mmol) in THF (7 mL), giving a deep red suspension. The reaction mixture was allowed to warm to room temperature and stirred for 1 h. Following removal of the volatiles under reduced pressure, the residue was triturated with hexane (10 mL) and dried *in vacuo* to afford a deep red solid. The product was extracted into toluene (3 × 5 mL), filtered and the combined filtrates were concentrated under reduced pressure. Cooling this solution to −20 °C produced red crystals of $[Fe_2(\mu\text{-}2)_2]$.(toluene) which were isolated by decantation and dried *in vacuo*. Total yield: 98 mg, 0.23 mmol (57%).

^{1}H NMR (400 MHz, C$_6$D$_6$, 298 K): δ_H 88.1 ($\Delta\nu_{\frac{1}{2}}$ = 39 Hz), 15.3 (v br), −46.1 (v br), −55.6 ($\Delta\nu_{\frac{1}{2}}$ = 182 Hz), −91.6 ($\Delta\nu_{\frac{1}{2}}$ = 225 Hz). ^{13}C NMR resonances were not observed due to the paramagnetic nature of $[Fe_2(\mu\text{-}2)_2]$. Anal. found (calcd for C$_{46}$H$_{48}$Fe$_2$N$_4$S$_4$·C$_7$H$_8$): C, 64.39 (64.79); H, 6.13 (5.64); N, 5.38 (5.60). IR (ATR): ν 1557, 1460, 1415, 1365, 1343, 1211 cm^{-1}. Magnetic susceptibility: (Evans method, C$_6$D$_6$, 298 K) μ_{eff} = 4.64μ_B per metal centre.

Synthesis and characterisation of [Co$_2$(μ-2)$_2$]

A Schlenk flask was charged with H$_2$**2** (50 mg, 0.13 mmol) and LiN(TMS)$_2$·THF (64 mg, 0.27 mmol). THF (5 mL) was added at −78 °C, affording a yellow suspension which was allowed warm to room temperature and stir for 1 h. The mixture was transferred *via* cannula to a pre-cooled −78 °C suspension of CoCl$_2$·THF$_{1.5}$ (32 mg, 0.14 mmol) in THF (7 mL), giving a green suspension. The reaction mixture was allowed to warm to room temperature and after stirring for 1 h appeared as a brown solution. Following removal of the volatiles under reduced pressure, the residue was triturated with hexane (10 mL) and dried *in vacuo* to afford a light brown solid. The product was extracted into toluene (3 × 5 mL), filtered and the combined filtrates were concentrated under reduced pressure. Cooling this solution to −20 °C produced brown crystals suitable for XRD analysis, which were isolated by decantation and dried *in vacuo*. Samples for bulk purity were obtained by addition of hexane to a saturated toluene solution at room temperature, which were isolated by decantation, washed with hexane and dried *in vacuo*. Total yield: 20 mg, 0.006 mmol (4%).

^{1}H NMR (400 MHz, C$_6$D$_6$, 298 K): δ_H 54.1 ($\Delta\nu_{\frac{1}{2}}$ = 21 Hz), 43.5 ($\Delta\nu_{\frac{1}{2}}$ = 18 Hz), −6.9 ($\Delta\nu_{\frac{1}{2}}$ = 124 Hz), −7.3 ($\Delta\nu_{\frac{1}{2}}$ = 97 Hz), −44.7 ($\Delta\nu_{\frac{1}{2}}$ = 90 Hz). ^{13}C NMR resonances were not observed due to the paramagnetic nature of [Co$_2$(μ-2)$_2$]. HRMS (ESI) *m/z* calcd for C$_{46}$H$_{48}$N$_4$S$_4$Co$_2$$^+$: 902.1426 [M]$^+$; found: 902.1429. Anal. found (calcd for C$_{46}$H$_{48}$Co$_2$N$_4$S$_4$·0.6C$_7$H$_8$): C, 62.53 (62.53); H, 5.37 (5.55); N, 5.43 (5.85). Satisfactory elemental analysis could not be obtained despite repeated attempts on freshly prepared samples, so data ±0.5% are reported. IR (ATR): ν 1557, 1470, 1419, 1367, 1349, 1213 cm^{-1}. Magnetic susceptibility: (Evans method, CDCl$_3$, 298 K) μ_{eff} = 3.85μ_B per metal centre.

Synthesis and characterisation of [Zn$_2$(μ-2)$_2$]

Method A/*via* protonolysis. A solution of ZnEt$_2$ (0.3 mL, 0.45 mmol, 1.5 M in toluene) was added to a solution of H$_2$**2** (114 mg, 0.29 mmol) in toluene (10 mL) at −78 °C, resulting in effervescence and a cloudy orange mixture, which was allowed to warm room temperature and stir for 1 h. The volatile components were removed under reduced pressure to afford a light yellow solid. The solid was suspended in Et$_2$O (6 mL) and THF was added (3 mL) until a yellow solution formed above insoluble material. The solution was filtered and stored at 4 °C, to afford the title compound as yellow microcrystals that were isolated and dried *in vacuo*. Yield: 30 mg, 0.10 mmol (23%).

Method B/*via* salt metathesis. A Schlenk flask was charged with H$_2$**2** (300 mg, 0.75 mmol) and LiN(TMS)$_2$·THF (300 mg, 0.75 mmol). THF (7 mL) was added at −78 °C, affording a yellow-orange suspension which was allowed warm to room temperature and stir for 1 h. The mixture was transferred *via* cannula to a pre-cooled −78 °C solution of ZnCl$_2$ (108 mg, 0.79 mmol) in THF (7 mL), giving a pale yellow suspension. The reaction mixture was allowed to warm to room temperature and stirred for 1 h. Following removal of the volatiles under reduced pressure, the residue was washed with hexane

(10 mL) and dried *in vacuo* to afford a colourless solid. The product was extracted into toluene (3 × 5 mL), filtered and the combined filtrates were concentrated under reduced pressure. Cooling this solution to −20 °C produced yellow crystals which were isolated by decantation and dried *in vacuo*. Yield: 39 mg, 0.10 mmol (11%).

^{1}H NMR (400 MHz, CDCl$_3$, 298 K): δ_H 6.92 (br, 4H, Ar C*H*), 6.61 (br, 4H, Ar C*H*), 6.12 (s, 2H, β-C*H*), 3.96 (s, 2H, C*H$_2$*), 2.40 (s, 6H, α-SCC*H$_3$*), 1.39 (s, 6H, α-NCC*H$_3$*). ^{13}C{^{1}H} NMR (100.5 MHz, C$_6$D$_6$, 298 K): δ_C 207.5 (*C*=S), 163.6 (α-N*C*CH$_3$), 139.7 (Ar *C$_Q$*−N), 135.6 (Ar *C$_Q$*−CH$_2$), 129.9 (Ar *C*H), 125.5 (Ar *C*H), 114.0 (β-*C*H), 41.0 (*C*H$_2$), 39.1 (α-S*C*CH$_3$), 21.5 (α-NC*C*H$_3$). ^{13}C{^{1}H} NMR (201.2 MHz, C$_6$D$_6$, 300 K, selected data): δ_C 173.5 (*C*=S), 172.7 (α-N*C*CH$_3$), 146.6 (Ar *C$_Q$*−N), 137.3 (Ar *C$_Q$*−CH$_2$), 128.4 (Ar *C*H), 123.6 (Ar *C*H), 119.4 (β-*C*H), 40.1 (*C*H$_2$), 35.9 (α-S*C*CH$_3$), 25.1 (α-NC*C*H$_3$). HRMS (ESI) *m/z* calcd for C$_{46}$H$_{49}$N$_4$S$_4$Zn$_2$$^+$: 917.1384 [M + H]$^+$; found: 917.1411; calcd for C$_{46}$H$_{48}$NaN$_4$S$_4$Zn$_2$$^+$: 939.1225 [M + Na]$^+$; found: 939.1203. Anal. found (calcd for C$_{46}$H$_{48}$N$_4$S$_4$Zn$_2$): C, 60.00 (60.32); H, 4.70 (5.28); N, 5.73 (6.12). Satisfactory elemental analysis could not be obtained despite repeated attempts on freshly prepared samples, so data ±0.6% are reported. IR (ATR): ν 1573, 1479, 1361, 1351, 1215 cm^{-1}.

Synthesis and characterisation of [Fe(3)$_2$]

A Schlenk flask was charged with H(**3**) (100 mg, 0.36 mmol) and KN(TMS)$_2$ (73 mg, 0.36 mmol). THF (3 mL) was added at −78 °C, affording a yellow-orange suspension which was allowed warm to room temperature and stir for 1 h. The mixture was transferred *via* cannula to a pre-cooled −78 °C suspension of FeCl$_2$·THF$_{1.5}$ (43 mg, 0.18 mmol) in THF (3 mL), resulting in a red suspension. The reaction mixture was allowed to warm to room temperature and stirred for 1 h, after which time the volatiles were removed under reduced pressure. The product was extracted into toluene (3 × 5 mL), filtered and then evaporated to dryness leaving the product as a red powder which was recrystallised from pentane at −20 °C to provide [Fe(**3**)$_2$] as red crystals. Total yield: 38 mg, 0.06 mmol (34%). ^{1}H NMR (400 MHz, C$_6$D$_6$, 298 K): δ_H 57.0 ($\Delta\nu_{\frac{1}{2}}$ = 1851 Hz), 20.3 ($\Delta\nu_{\frac{1}{2}}$ = 67 Hz), 15.1 ($\Delta\nu_{\frac{1}{2}}$ = 230 Hz), 14.8 ($\Delta\nu_{\frac{1}{2}}$ = 69 Hz), −2.4 ($\Delta\nu_{\frac{1}{2}}$ = 298 Hz), −4.7 ($\Delta\nu_{\frac{1}{2}}$ = 235 Hz), −12.7 ($\Delta\nu_{\frac{1}{2}}$ = 230 Hz), −26.8 ($\Delta\nu_{\frac{1}{2}}$ = 169 Hz), −36.8 ($\Delta\nu_{\frac{1}{2}}$ = 209 Hz), −41.2 ($\Delta\nu_{\frac{1}{2}}$ = 252 Hz), −64.7 ($\Delta\nu_{\frac{1}{2}}$ = 1807 Hz), −77.2 ($\Delta\nu_{\frac{1}{2}}$ = 498 Hz). ^{13}C NMR resonances were not observed due to the paramagnetic nature of [Fe(**3**)$_2$]. Anal. found (calcd for C$_{34}$H$_{48}$FeN$_2$S$_2$): C, 67.41 (67.53); H, 8.11 (8.00); N, 4.57 (4.63). Magnetic susceptibility: (Evans method, C$_6$D$_6$, 298 K) μ_{eff} = 4.58μ_B per metal centre.

Synthesis and characterisation of [Co(3)$_2$]

To a precooled solution of H(**3**) (200 mg, 0.72 mmol) in THF (5 mL) at −78 °C, was added ^{n}BuLi solution (2.5 M in hexanes, 0.30 mL, 0.76 mmol), affording a yellow mixture which was allowed warm to room temperature and stirred for 1 h. To which was added a precooled solution of CoCl$_2$·THF$_{1.5}$ (92 mg, 0.39 mmol) in THF (7 mL) at −78 °C, resulting in a green suspension which rapidly turned brown. The mixture was warmed

to room temperature and stirred for 2 h, and the volatiles were removed under reduced pressure. The product was extracted into toluene (3 × 3 mL), filtered and then evaporated to dryness leaving the product as a brown powder which was recrystallised from Et$_2$O at −20 °C to provide [Co(**3**)$_2$] as brown crystals. Total yield: 98 mg, 0.17 mmol (44%). ^{1}H NMR (400 MHz, C$_6$D$_6$, 298 K): δ_H 43.4 ($\Delta\nu_{\frac{1}{2}}$ = 1072 Hz), 16.7 ($\Delta\nu_{\frac{1}{2}}$ = 48 Hz), 10.2 ($\Delta\nu_{\frac{1}{2}}$ = 106 Hz), 9.2 ($\Delta\nu_{\frac{1}{2}}$ = 75 Hz), −0.3 ($\Delta\nu_{\frac{1}{2}}$ = 89 Hz), −4.2 ($\Delta\nu_{\frac{1}{2}}$ = 198 Hz), −7.8 ($\Delta\nu_{\frac{1}{2}}$ = 159 Hz), −9.2 ($\Delta\nu_{\frac{1}{2}}$ = 115 Hz), −15.0 ($\Delta\nu_{\frac{1}{2}}$ = 113 Hz), −24.8 ($\Delta\nu_{\frac{1}{2}}$ = 32 Hz), −42.0 ($\Delta\nu_{\frac{1}{2}}$ = 685 Hz), −74.0 ($\Delta\nu_{\frac{1}{2}}$ = 252 Hz). ^{13}C NMR resonances were not observed due to the paramagnetic nature of [Co(**3**)$_2$]. Anal. found (calcd for C$_{34}$H$_{48}$CoN$_2$S$_2$): C, 67.20 (67.19); H, 8.05 (7.96); N, 4.77 (4.61). Magnetic susceptibility: (Evans method, C$_6$D$_6$, 298 K) μ_{eff} = 3.83μ_B per metal centre.

Synthesis and characterisation of [Zn(3)$_2$]

A Schlenk flask was charged with H(**3**) (275 mg, 1.0 mmol) dissolved in toluene (10 mL) cooled to −78 °C, ZnEt$_2$ (1.5 M, 0.33 mL, 0.5 mmol) was added dropwise, and effervescence was observed, affording an orange solution, which was allowed warm to warm to room temperature and stir for 24 h, affording a light yellow solution. Following removal of the volatiles under reduced pressure, the yellow residue was washed with hexane (3 × 2 mL) and dried *in vacuo* to provide [Zn(**3**)$_2$] as beige powder. Total yield: 182 mg, 0.30 mmol (59%). ^{1}H NMR (400 MHz, C$_6$D$_6$, 298 K): δ_H 7.19 (m, 2H, Ar *p*-C*H*), 7.13–7.08 (m, 4H, 2 × Ar *m*-C*H*), 5.85 (s, 2H, β-C*H*), 3.16 (sept, $^3J_{HH}$ = 6.6 Hz, 2H, ^{i}Pr C*H*), 3.08 (sept, $^3J_{HH}$ = 6.6 Hz, 2H, ^{i}Pr C*H*), 1.96 (s, 6H, α-SCC*H$_3$*), 1.53–1.50 (m, 12H, α-NCC*H$_3$* and ^{i}Pr C*H$_3$* overlapping), 1.26 (d, $^3J_{HH}$ = 6.8 Hz, 6H, ^{i}Pr C*H$_3$*), 1.10 (d, $^3J_{HH}$ = 6.7 Hz, 6H, ^{i}Pr C*H$_3$*), 0.98 (d, $^3J_{HH}$ = 6.8 Hz, 6H, ^{i}Pr C*H$_3$*). ^{13}C{^{1}H} NMR (100.5 MHz, C$_6$D$_6$, 298 K): δ_C 174.3 (*C*=S), 169.3 (α-N*C*CH$_3$), 144.6 (Ar *i*-C$_Q$), 141.8 (Ar *o*-C$_Q$), 140.0 (Ar *C*$_Q$), 126.4 (Ar *C*H), 124.9 (Ar *C*H), 123.1 (Ar *C*H), 119.1 (β-*C*H), 34.8 (α-S*C*CH$_3$), 29.2 (^{i}Pr *C*H), 28.5 (^{i}Pr *C*H), 25.7 (α-NC*C*H$_3$), 25.0 (^{i}Pr *C*H$_3$), 24.9 (^{i}Pr *C*H$_3$), 24.4 (^{i}Pr *C*H$_3$), 23.9 (^{i}Pr *C*H$_3$). Anal. found (calcd for C$_{34}$H$_{48}$N$_2$S$_2$Zn): C, 66.59 (66.48); H, 7.79 (7.88); N, 4.36 (4.56).

Author contributions

Conceptualisation, A. F. R. K., J. A., J. S.; methodology, J. A., J. S., A. F. R. K.; validation, J. A., J. S., A. F. R. K.; formal analysis, J. A., J. S., K. S., A. F. R. K.; investigation, J. A., J. S., A. F. R. K., K. S.; writing – original draft, A. F. R. K., J. A., J. S.; writing – review & editing, A. F. R. K., J. A., J. S.; visualisation, A. F. R. K., J. S., J. A., K. S.; supervision, A. F. R. K.; project administration, A. F. R. K.; funding acquisition, A. F. R. K.

Data availability

The data supporting this article, including crystallographic details, additional NMR and IR spectroscopic data, HRMS, cyclic voltammetry, and DFT calculations, have been included as part of the ESI.† The raw data for all the figures are openly available on Zenodo: **https://doi.org/10.5281/zenodo.13858221**. Crystallographic data for compounds H$_2$**2**, [M$_2$(µ-**2**)$_2$], and [M(**3**)$_2$] (M = Fe, Co, and Zn) have been deposited at the CCDC under 2330325–2330332.†

Conflicts of interest

There are no conflicts to declare.

Acknowledgements

References

1 J. Campos, *Nat. Rev. Chem.*, 2020, **4**, 696–702.
2 N. P. Mankad, *Chem. – Eur. J.*, 2016, **22**, 5822–5829.
3 J. Park and S. Hong, *Chem. Soc. Rev.*, 2012, **41**, 6931–6943.
4 I. Bratko and M. Gómez, *Dalton Trans.*, 2013, **42**, 10664–10681.
5 G. W. J. Everett and R. H. Holm, *J. Am. Chem. Soc.*, 1965, **87**, 2117–2127.
6 S. Debnath, N. Arulsamy and M. P. Mehn, *Inorg. Chim. Acta*, 2019, **486**, 441–448.
7 L.-M. Tang, J.-Q. Wu, Y.-Q. Duan, L. Pan, Y.-G. Li and Y.-S. Li, *J. Polym. Sci., Part A: Polym. Chem.*, 2008, **46**, 2038–2048.
8 H.-Y. Wang, J. Zhang, X. Meng and G.-X. Jin, *J. Organomet. Chem.*, 2006, **691**, 1275–1281.
9 D. H. Gerlach and R. H. Holm, *Inorg. Chem.*, 1970, **9**, 588–594.
10 R. H. Holm, G. W. Everett Jr. and A. Chakravorty, *Progress in Inorganic Chemistry*, 1966, pp. 83–214.
11 R. Kretschmer, *Chem. – Eur. J.*, 2019, **115**, 22–28.
12 M. Kopf, D. Varech, J. Tuchagues and I. Artaud, *J. Chem. Soc., Dalton Trans.*, 1998, 991–998.

13 M. Gennari, M. Retegan, S. Debeer, J. Pécaut, F. Neese, M. N. Collomb and C. Duboc, *Inorg. Chem.*, 2011, **50**, 10047–10055.

14 L. Wang, M. Gennari, F. G. Cantu Reinhard, J. Gutierrez, A. Morozan, C. Philouze, S. Demeshko, V. Artero, F. Meyer, S. P. de Visser and C. Duboc, *J. Am. Chem. Soc.*, 2020, **141**, 8244–8253.

15 M. Gennari, B. Gerey, N. Hall, J. Pécaut, H. Vezin, M. N. Collomb, M. Orio and C. Duboc, *Dalton Trans.*, 2012, **41**, 12586–12594.

16 M. Gennari, J. Pécaut, S. Debeer, F. Neese, M. N. Collomb and C. Duboc, *Angew. Chem., Int. Ed.*, 2011, **50**, 5662–5666.

17 J. Dömer, J. C. Slootweg, F. Hupka, K. Lammertsma and F. E. Hahn, *Angew. Chem., Int. Ed.*, 2010, **49**, 6430–6433.

18 D. Lewing, H. Koppetz and F. E. Hahn, *Inorg. Chem.*, 2015, **54**, 7653–7659.

19 Z. S. Wu, J. T. Hsu, C. C. Hsieh and Y. C. Horng, *Chem. Commun.*, 2012, **48**, 3436–3438.

20 J. Rangel-Garcia, C. E. Rivas, O. Serrano and C. Cristobal, *Eur. J. Inorg. Chem.*, 2024, e202400118.

21 T. Tokumitsu and T. Hayashi, *Bull. Chem. Soc. Jpn.*, 1981, **54**, 2348–2351.

22 M. Fujiwara, H. Wakita, T. Matsushita and T. Shono, *Bull. Chem. Soc. Jpn.*, 1990, **63**, 3443–3449.

23 V. M. Rendón-López, Á. J. A. Castro, J. C. Alvarado-Monzón, C. Cristóbal, G. G. Gonzalez, S. G. Montiel, O. Serrano and J. A. López, *Polyhedron*, 2019, **162**, 207–218.

24 D. O. González-Ábrego, G. Sánchez-Cabrera, F. J. Zuno-Cruz, J. A. Rodriguez, J. G. Alvarado-Rodríguez, N. Andrade-López, J. A. López, C. Cristóbal and G. González-García, *Inorg. Chim. Acta*, 2021, **514**, 120000.

25 V. S. S. Penki, Y.-L. Chang, H.-Y. Chen, Y.-T. Chu, Y.-T. Kuo, D. P. P. Dorairaj, S. Sudewi, S. Ding and S. C. N. Hsu, *Dalton Trans.*, 2023, 1772.

26 P. K. Ganta, M. R. Teja, R. Kamaraj, Y. Tsai, Y. Chu, A. Sambandam, Y. Lai, S. Ding and H. Chen, *Organometallics*, 2023, **42**, 3405–3417.

27 J. Rangel-Garcia, C. E. Rivas, J. Campos, O. Serrano and C. Cristobal, *Eur. J. Inorg. Chem.*, 2024, e202400355.

28 M. L. Clapson, C. S. Durfy, D. Facchinato and M. W. Drover, *Cell Rep. Phys. Sci.*, 2023, 101548.

29 R. Cini, A. Cinquantini, P. Oriolli and M. Sabat, *Inorg. Chim. Acta*, 1980, **41**, 151–154.

30 R. Cini, A. Cinquantini, P. L. Orioli, C. Mealli and M. Sabat, *Can. J. Chem.*, 1984, **62**, 2908–2913.

31 M. J. E. Hewlins, *J. Chem. Soc., Dalton Trans.*, 1975, 429–432.

32 T. G. Takhirov, O. A. D'yachenko, D. B. Tagiev, A. L. Nivorozhkin, M. S. Korobov, R. Y. Olekhnovich, L. E. Nivorozhkin and V. I. Minkin, *Koord. Khim.*, 1991, **17**, 711–719.

33 C. Helling, J. C. Farmer, C. Wölper, R. Kretschmer and S. Schulz, *Organometallics*, 2023, **42**, 72–80.

34 O. Kysliak, H. Görls and R. Kretschmer, *J. Am. Chem. Soc.*, 2021, **143**, 142–148.

35 M. E. Desat and R. Kretschmer, *Dalton Trans.*, 2019, **48**, 17718–17722.

36 Y.-C. Tsai, *Coord. Chem. Rev.*, 2012, **256**, 722–758.

37 H. K. Luo and H. Schumann, *J. Mol. Catal. A: Chem.*, 2005, **227**, 153–161.

38 I. I. Oleinik, I. V. Oleinik, S. S. Ivanchev and G. A. Tolstikov, *Russ. J. Org. Chem.*, 2009, **45**, 528–535.

39 S. Budagumpi, Y. Liu, H. Suh and I. Kim, *J. Organomet. Chem.*, 2011, **696**, 1887–1894.

40 B. K. Bahuleyan, K. J. Lee, S. H. Lee, Y. Liu, W. Zhou and I. Kim, *Catal. Today*, 2011, **164**, 80–87.

41 S. S. Ivanchev, A. V. Yakimansky, N. I. Ivancheva, I. I. Oleinik and G. A. Tolstikov, *Eur. Polym. J.*, 2012, **48**, 191–199.

42 S. Kong, K. Song, T. Liang, C. Y. Guo, W. H. Sun and C. Redshaw, *Dalton Trans.*, 2013, **42**, 9176–9187.

43 L. Xiao, Y. Zhao, S. Qiao, Z. Sun, O. Santoro and C. Redshaw, *Dalton Trans.*, 2020, **49**, 1456–1472.

44 P. E. Kruger, N. Martin and M. Nieuwenhuyzen, *J. Chem. Soc., Dalton Trans.*, 2001, 1966–1970.

45 M. J. Hannon, C. L. Painting and N. W. Alcock, *Chem. Commun.*, 1999, **2**, 2023–2024.

46 M. W. Lehenmeier, S. Kissling, P. T. Altenbuchner, C. Bruckmeier, P. Deglmann, A.-K. Brym and B. Rieger, *Angew. Chem., Int. Ed.*, 2013, **52**, 9821–9826.

47 D. Ruiz Plaza, J. C. Alvarado-Monzón, G. A. Andreu de Riquer, G. González-García, H. Höpfl, L. M. de León-Rodríguez and J. A. López, *Eur. J. Inorg. Chem.*, 2016, 874–879.

48 V. S. S. Penki, Y. T. Chu, H.-Y. Chen, S. Sudewi, C.-H. Li, G. G. Huang and S. C. N. Hsu, *Dalton Trans.*, 2024, **53**, 13160–13173.

49 K. Kumar Chouhan, P. Nad and A. Mukherjee, *Chem. – Asian J.*, 2023, **18**, e202300738.

50 C. O'Connor, D. C. Lawlor, C. Robinson, H. Müller-Bunz and A. D. Phillips, *Organometallics*, 2018, **37**, 1860–1875.

51 F. H. Allen, O. Kennard, D. G. Watson and L. Brammer, *J. Chem. Soc., Perkin Trans. 2*, 1987, S1–S19.

52 D. M. Granum, P. J. Riedel, J. A. Crawford, T. K. Mahle, C. M. Wyss, A. K. Begej, N. Arulsamy, B. S. Pierce and M. P. Mehn, *Dalton Trans.*, 2011, **40**, 5881–5890.

53 D. F. J. Piesik, S. Range and S. Harder, *Organometallics*, 2008, **27**, 6178–6187.

54 D. F. J. Piesik, R. Stadler, S. Range and S. Harder, *Eur. J. Inorg. Chem.*, 2009, 3569–3576.

55 B. Rösch, T. X. Gentner, J. Eyselein, A. Friedrich, J. Langer and S. Harder, *Chem. Commun.*, 2020, **318**, 1754.

56 P. Rinke, H. Görls and R. Kretschmer, *Inorg. Chem.*, 2021, **60**, 5310–5321.

57 J. Wang, H. Sun, Y. Yao, Y. Zhang and Q. Shen, *Polyhedron*, 2008, **27**, 1977–1982.

58 H. Kawaguchi and T. Matsuo, *Chem. Commun.*, 2002, 958–959.

59 S. Abbina, V. K. Chidara, S. Bian, A. Ugrinov and G. Du, *ChemistrySelect*, 2016, **1**, 3175–3183.

60 N. Yoshida, K. Ichikawa and M. Shiro, *J. Chem. Soc., Perkin Trans. 2*, 2000, 17–26.

61 A. P. Paneerselvam, S. S. Mishra and D. K. Chand, *J. Chem. Sci.*, 2018, **130**, 1–18.

62 L. Yang, D. R. Powell and R. P. Houser, *Dalton Trans.*, 2007, 955–964.

63 C. R. Martinez and B. L. Iverson, *Chem. Sci.*, 2012, **3**, 2191–2201.

64 R.-M. Ma, S.-F. Sun and F. Bao, *Acta Crystallogr., Sect. E: Struct. Rep. Online*, 2006, **62**, m3170–m3171.

65 J. I. Lee, T. Y. Lee, L. C. Chang, C. Y. Lin, H. M. Lee, L. Hung, A. Datta and J. H. Huang, *J. Mol. Struct.*, 2009, **929**, 207–212.

66 B. R. M. Lake and M. P. Shaver, *Dalton Trans.*, 2016, **45**, 15840–15849.

67 M. R. Elsby, K. Ghostine, U. K. Das, B. M. Gabidullin and R. T. Baker, *Organometallics*, 2019, **38**, 3844–3851.

68 R. C. R. Bottini, R. A. Gariani, C. O. De Cavalcanti, F. De Oliveira, N. L. G. De Da Rocha, D. Back, E. S. Lang, P. B. Hitchcock, D. J. Evans, G. G. Nunes, F. Simonelli, E. L. De Sá and J. F. Soares, *Eur. J. Inorg. Chem.*, 2010, 2476–2487.

69 N. Govindaswamy, D. A. Quarless and S. A. Koch, *J. Am. Chem. Soc.*, 1995, **117**, 8468–8469.

70 G. Mugesh, H. B. Singh and R. J. Butcher, *Eur. J. Inorg. Chem.*, 1999, 1229–1236.

71 J. C. Jeffery, C. S. G. Moore, E. Psillakis, M. D. Ward and P. Thornton, *Polyhedron*, 1995, **14**, 599–604.

72 M. B. Robin and P. Day, *Adv. Inorg. Chem. Radiochem.*, 1968, **10**, 247–422.

73 J. Evans, *J. Chem. Soc.*, 1959, 2003–2005.

74 E. M. Schubert, *J. Chem. Educ.*, 1992, **69**, 62.

75 L. Zhang, L. Xiang, Y. Yu and L. Deng, *Inorg. Chem.*, 2013, **52**, 5906–5913.

76 F. Téllez, A. Flores-Parra, N. Barba-Behrens and R. Contreras, *Polyhedron*, 2004, **23**, 2481–2489.

77 W. P. Leung, Y. C. Chan and T. C. W. Mak, *Eur. J. Inorg. Chem.*, 2013, 6103–6110.

78 C. W. Bauschlicher, Jr., S. R. Langhoff, H. Partridge and L. A. Barnes, *J. Chem. Phys.*, 1989, **91**, 2399–2411.

79 A. J. H. Wachters, *J. Chem. Phys.*, 1970, **52**, 1033–1036.

80 M. Bühl and H. Kabrede, *J. Chem. Theory Comput.*, 2006, **2**, 1282–1290.

81 M. Bühl, C. Reimann, D. A. Pantazis, T. Bredow and F. Neese, *J. Chem. Theory Comput.*, 2008, **4**, 1449–1459.

82 A. A. Danopoulos, D. Pugh, H. Smith and J. Saßmannshausen, *Chem. – Eur. J.*, 2009, **15**, 5491–5502.

83 D. J. Cooke, J. M. Cross, R. V. Fennessy, L. P. Harding, C. R. Rice and C. Slater, *Chem. Commun.*, 2013, **49**, 7785–7787.

84 A. Bilyk, M. M. Harding, P. Turner and T. W. Hambley, *J. Chem. Soc., Dalton Trans.*, 1994, 2783–2790.

85 M. J. Hannon, C. L. Painting, A. Jackson, J. Hamblin and W. Errington, *Chem. Commun.*, 1997, 1807–1808.

86 M. Albrecht, *Chem. Rev.*, 2001, **101**, 3457–3498.

87 S. M. Mansell, N. Kaltsoyannis and P. L. Arnold, *J. Am. Chem. Soc.*, 2011, **133**, 9036–9051.